sciendo

Polish Journal of Chemical Technology, 26, 4, 87—96, 10.2478/pjct-2024-0044

Radial mixing in horizontal aerated tubular reactor

Mateusz R. Prończuk*

Faculty of Chemical Engineering and Technology, Cracow University of Technology,
ul. Warszawska 24, Kraków 31-155, Poland
**Corresponding author: e-mail:* mateusz.pronczuk@pk.edu.pl

The article discusses radial mixing in a Horizontal Aerated Tubular Reactor (HATR). The study aimed to experimentally investigate mixing in HATR by determining mixing time, liquid circulation time, and Peclet number values, which measure the ratio of advective to diffusive transport rates. The experimental setup included a transparent tube for observing fluid mixing and a color tracer was used for visualizing mixing. Mixing and circulation times were determined using non-intrusive optical method. The experimentally determined circulation time was in the range of 3÷6.5 s, and the mixing time was in the range of 5÷20 s. The results suggested that fluid flow structure in HATR was closer to plug flow rather than ideal mixing, as indicated by high Peclet numbers (20÷45).

Keywords: horizontal aerated tubular reactor, radial dispersion, radial mixing, mixing time, optical measurements.

INTRODUCTION

Aerobic microbiological processes can be carried out in many different types of apparatus. The selection of the appropriate instrument used to conduct microbial processes depends on many factors, such as the kinetics of the microbial reaction, hydrodynamics and the scale of production[1]. In biotechnology, continuous stirred tank reactors are the most popular. These are relatively simple devices, and the intensive mixing helps to rapidly distribute the components throughout the mixture, making the concentration field in the device homogeneous. This is particularly advantageous when a strong acid or strong base is used to regulate the pH of the reaction environment. Besides, making the assumption of complete mixing allows simplifying process calculations[2].

However, such devices also have a number of disadvantages. The mixing itself requires the supply of a considerable amount of energy. The use of an agitator also requires proper sealing and bearing of the agitator shaft, which can be a concern when running sterile processes, as any seal has the potential to contaminate the reaction environment if it fails. In addition, the high shear stresses caused by the rotation of the impeller blades can damage delicate biomass cells[1].

An alternative to tank reactors are tubular reactors. They do not have the disadvantages mentioned above, and due to their slender design, the flow structure is closer to plug flow than to complete mixing. Tubular reactors usually have no moving parts, making them virtually unattended[1]. In such apparatuses, there is a certain concentration distribution along the length of the tubular reactor. As a result, such devices are also less susceptible to the inhibition by the product of the reaction, since the high concentration of the product causing a reduction in the reaction rate occurs only in a certain part of the apparatus[3].

Tubular reactors often allow higher conversion levels than CSTRs for the same reactor volume or residence time. Since there is some distribution of reaction substrate concentration along the reactor, the reaction rate changes throughout the length of the apparatus. Higher substrate concentrations at the entrance of the apparatus result in a higher driving force for the reaction, therefore the reaction rate at the reactor inlet can be higher than in an apparatus with complete mixing. This may contribute to increased conversion e.g. for reactions without inhibition and reactions with product inhibition[4] (since the concentration of product is lower in the initial part of the apparatus, so the effect of inhibition will be weaker there), but on the other hand, for reactions with substrate inhibition, the conversion in a tubular reactor may be lower than in a CSTR reactor of identical volume. Tubular reactors also have a much higher surface-to-volume ratio compared to CSTRs, so biofilm can be deposited on the pipe walls, whose presence prevents the phenomenon of biomass washout from the reactor, even at relatively high flow rates[1].

Tubular reactors for aerobic processes can have many different designs. We can find a broad review of horizontal tubular bioreactors in the article by Šantek et al. (2006)[1]. The simplest design is an apparatus in the form of a tube laid horizontally, usually in the form of a loop. Such tubular reactors can also be coupled with other devices, such as a bubble column, to which a loop of pipes is connected at the bottom and top. The bubble column serves a dual role here; in addition to aeration, the introduction of air into the column lowers the average density of the fluid in the apparatus, which in turn forces the fluid to circulate, similar to the airlift apparatus.

Other ways of modifying a tubular apparatus for oxygen processes involve introducing some kind of mixing device inside the tube, for example, in the form of rotating disks[5] or cylinders[6]. On the surface of the moving elements of the apparatus, microorganism cells are deposited. As the moving elements rotate slowly, they are periodically submerged below the water surface, from where the microorganisms take up nutrients, and then raised above the water surface, from where oxygen is absorbed. In addition, the moving elements intensify mixing in the direction perpendicular to the axis of the reactor, thus helping to reduce longitudinal mixing, so we can consider the flow in such an apparatus as close to a plug flow[1].

Another modification of a tubular reactor for the purpose of aerobic processes may be the Horizontal Aerated Tubular Reactor (HATR)[3]. Such a device has been studied extensively by Moser. In the design discussed here, air is introduced at the bottom of the

horizontal reactor tube. Aeration can be accomplished by holes drilled in the bottom of the apparatus tube or by introducing a gas distributor, usually in the form of a small-diameter porous tube along the length of the reactor. In this way it was possible to minimize the impact of one of the biggest disadvantages of aerobic processes, which is the possibility of oxygen deficiency in the reaction environment. The reactor itself has no moving parts, which also further increases the reliability of such a device[3].

In this type of reactor, Moser[3] carried out a microbial ethanol synthesis reaction using *Zymomonas mobilis* and compared the results obtained with CSTR. The study showed that in order to achieve the same degree of conversion, it was necessary to use a CSTR with a total volume greater than that of the tubular reactor. The difference was greater the higher the substrate conversion level, for a conversion level of 98% the required volume of the tubular reactor was about 40% less than the volume of the tank reactor.

The literature also contains reports on mixing in HATR. According to the results of Moser's research, such a reactor is characterized by a flow very close to plug flow[3]. Experimentally determined values of the Peclet number for longitudinal dispersion in the apparatus were in the range of 20÷80. With such a high value of Peclet numbers, the flow in the apparatus can be treated with high accuracy as a plug flow. Gas bubbles rising in the plane of symmetry of the apparatus cause strong mixing in the cross-section of the apparatus, resulting in conditions similar to the model one-dimensional plug flow[3].

Unfortunately, no studies describing radial dispersion in the apparatus can be found in the literature. A one-dimensional flow model with longitudinal dispersion assumes that the fluid in the cross-section of the apparatus is perfectly mixed, however, high Peclet number values for axial flow may suggest that mixing in the cross-section of the apparatus is far from ideal. The purpose of the present study is to experimentally investigate mixing in the HATR. For this purpose, mixing time, liquid circulation time and Peclet number values in the apparatus were determined as a function of the volumetric flow rate of the gas in the apparatus.

MATERIALS AND METHODS

Experimental setup

A schematic drawing of the test stand is shown in Fig. 1. The investigated Horizontal Aerated Tube Reactor (1 in Fig. 1) was made of a transparent poly(methyl methacrylate) (PMMA) tube with a length L_r = 2 m of and an inner diameter of D = 80 mm. Flanges also made of PMMA were attached to the ends of the tube. Thanks to this design of the apparatus, it was possible to record the flow behavior inside the apparatus. The pipe was filled with water to a height equal to half the diameter. Below the surface of the liquid, near the bottom wall of the apparatus, there was a gas distributor (2 in Fig. 1). The role of the distributor was played by an aluminum tube with an outer diameter of d_o = 10 mm placed at the bottom of the apparatus, in the upper part of the tube holes with a diameter of d = 1 mm were drilled, spaced evenly by l = 20 mm over a length of L = 1 m. In the center of the tube was a nozzle for the tracer injection (3 in Fig. 1). Air was supplied from both sides of the gas distributor to ensure that the gas was distributed as evenly as possible throughout its length. The volumetric flow rate of the injected air was measured using a rotameter (4 in Fig. 1), and was adjusted using a needle valve (5 in Fig. 1) located just upstream of the rotameter. Pressurized air was supplied to the system using an air compressor (6 in Fig. 1). A camera (7 in Fig. 1) was placed on the extension of the apparatus centerline, and was used to record the flow of the tracer during the experiments.

In order to ensure the most uniform flow of the tracer, it was introduced through the tube with two coaxial holes drilled symmetrically on the side wall of the tube (the hole at the end of the tube was sealed). During the experiments, the holes were arranged so that the tracer was introduced symmetrically on both sides of

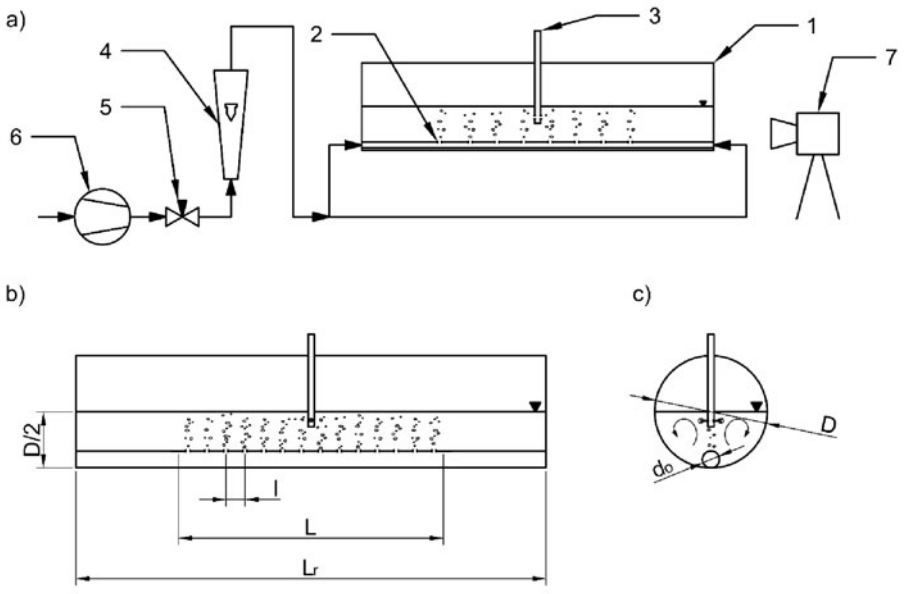

Figure 1. Schematic drawing of the: a) experimental setup, b) axial cross section of the HATR, c) radial cross section of the HATR (drawings not to scale)

the apparatus. In addition, the tracer injection point was placed between the two holes in the gas distributor, at a height of about 10 mm below the surface of the liquid, so that the tracer was introduced in the same direction as the local liquid flow.

As mentioned earlier, air was used as the gas phase. The liquid phase was tap water at a temperature of about 15 °C. Blue ink was used as a color tracer. Too high concentration of the color tracer caused oversaturation of colors on the recorded video, so that the tracer's apparent concentration exceeded the maximum measurable level for most of the experiment. Since the color of the ink was too intense, it was diluted for the experiment. The 100-fold dilution of the ink allowed its concentration to be measured over a wide enough range, and allowed the measurement of its concentration to maintain satisfactory resolution.

High-speed IDS uEye camera model IU-3130CP-C-HQ was used in the experiments. The camera has a sensor with a resolution of 800x600 pixels, and allows recording color video at a maximum rate of 396 fps at full resolution. The camera was equipped with a Tamron HB35 lens with a focal length of 35 mm (f/2.1 to f/22). In the experiments, video was recorded at a reduced resolution of 120x120 pixels, which allowed the video frame rate to be increased to 500 fps.

Video recording was carried out using IDS Camera Suite software (version 4.94) provided by the camera manufacturer. Data analysis, image processing and numerical calculations were carried out using Mathworks Matlab software (version R2024a).

Data analysis

To determine the intensity of radial dispersion in the apparatus, experiments were carried out by injecting a colored tracer into the center of the apparatus and recording the mixing of the tracer with the fluid in the apparatus until the concentration field of the tracer became uniform across the cross section. A camera equipped with a color sensor was used for the study. The color information of each pixel in the image is stored in the RGB color space, so each pixel of the image has saturation information of the three primary colors: red, green and blue. In order to analyze the results obtained, the image was converted to grayscale. This made it possible to take into account the influence of all three basic color components, and a change in the concentration of the tracer was interpreted as a change in the brightness of the pixels in the image.

Initially, image analysis looked at the change in brightness of individual image pixels. However, this approach turned out to be faulty, as the results obtained were subject to a considerable amount of measurement noise. The brightness of individual pixels often changed quite significantly between successive frames of the recorded image. The reason for this was not only the measurement noise caused by the operation of the CCD sensor itself, but primarily the inhomogeneous structure of the tracer stream, which was caused by the presence of vortices turbulently mixing the tracer streams with clean water. In order to minimize fluctuations in image brightness, it was decided to analyze not individual pixels, but larger areas. For this purpose, the recorded image frame was

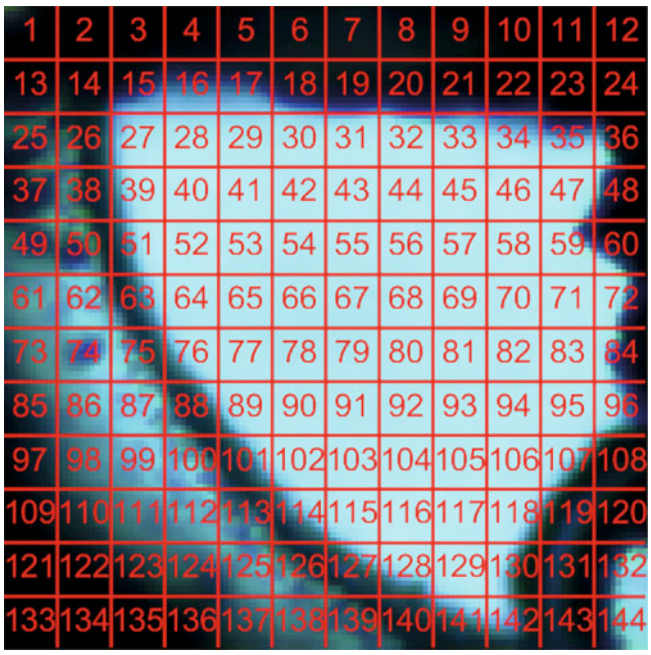

Figure 2. Example of a frame from the recorded video with image divided into 144 zones of a size of 10x10 pixels

divided into smaller fragments of 10x10 pixels, resulting in a total of 144 sub-areas (see Fig. 2). For each of these areas, the brightness was averaged over all the pixels obtained, resulting in results with much less measurement noise.

The film frame was square in shape, however, the area where tracer mixing was studied was in the shape of a 1/4 section of a circle, so not all 144 zones were analyzed. Areas outside the studied geometry were omitted, as well as areas on the edges of the frame that were located near the surface or in the immediate vicinity of flowing gas bubbles. Both the surface of the bubbles and the free surface of the liquid were in constant motion, so that the light could be totally reflected internally, which in turn manifested itself in the presence of dark spots in the image, such as in the area of the flowing bubble. Such a darker zone could be misinterpreted as an area containing a high concentration of tracer.

The resulting films made it possible to determine the brightness distribution in the image. For the purpose of analyzing the videos, however, the distribution of the concentration of the tracer is needed. The tracer introduced into the transparent liquid layer caused a decrease in the brightness of the image, and the change in brightness depended on the tracer concentration. To determine its concentration, Beer-Lambert's law (1) was used[7]:

$$A = \log\frac{I_0}{I} = \varepsilon l c \tag{1}$$

where:
A – absorbance, [–]
I_0 – the intensity of light passing through the sample before tracer injection, [W]
I – the intensity of light passing through the sample after tracer injection, [W]
ε – molar absorption coefficient, [m^2/mol]
l – length of the absorbing layer, [m]
c – tracer concentration, [mol/m^3]

The intensity of light passing through the sample is directly proportional to the brightness, so the brightness of the image can be used directly in equation (1). Equation (1) shows that the concentration of the tracer is proportional to the absorbance. The molar absorption coefficient, ε, actually only depends on the type of substance, and the length of the absorbing layer, l, was constant during the experiments, so we can write a simplified equation (2):

$$c = CA = C \log \frac{B_0}{B} \tag{2}$$

where:
C – constant depending on the molar absorption coefficient and the length of the absorbing layer, [mol/m^3]
B_0 – brightness of the image before tracer injection, [–]
B – brightness of the image after tracer injection, [–]

For the analysis, however, it is more convenient to use dimensionless concentrations. It can be determined from the momentary tracer concentration, the initial tracer concentration and the tracer concentration after total mixing (3):

$$\beta(t) = \frac{c(t) - c_0}{c_\infty - c_0} \tag{3}$$

where:
$\beta(t)$ – dimensionless tracer concentration, [–]
$c(t)$ – tracer concentration, [mol/m^3]
c_0 – initial tracer concentration, [mol/m^3]
c_∞ – tracer concentration after complete mixing, [mol/m^3]

An equation of this form is often used to describe the impulse response of a system with full circulation. When conducting tracer experiments, it is often impossible to directly measure the concentration of the tracer. Some physical quantity related to its concentration, such as light absorbance, is therefore measured. The apparent concentration of the tracer can then be higher than the actual concentration, since the absorbance for pure water (even distilled water) is always higher than zero, and light passing through a sample of even pure water will always be absorbed to some level. It is therefore necessary to reduce the results of instantaneous tracer concentration measurements by the measured apparent initial tracer concentration in the instrument. Once the tracer is completely mixed with the fluid in the apparatus, its concentration is fixed. Dividing the instantaneous concentration of the tracer by the concentration after complete mixing, we get a dimensionless quantity telling us how many times concentration was greater than the final concentration. With this methodology, we can compare the results of experiments that were conducted for a different initial concentration of tracer or different amounts of tracer introduced. Such normalized equation is often used in tracer studies and was used by, e.g.: Murakami et al.[9], Verlaan et al.[10] or Gavrilescu and Tudose[11].

The initial dimensionless concentration was equal to 0, since only water was present in the apparatus initially. The concentration after complete mixing was also determined from the recorded videos based on the average absorbance in the last 100 frames of the recorded video. As can easily be seen, if we combine equations (2) and (3), in the resulting equation the constant used to calculate the concentration, C, can be excluded in both the numerator and denominator of the right-hand side of equation (3), and can then be truncated. Thus, the dimensionless concentration can be calculated without knowing the value of the molar absorption coefficient, which allows for a significant simplification of the calculation.

Based on the obtained distributions of tracer concentration as a function of the time of the experiment, it was possible to determine the tracer circulation time, τ, and the mixing time, t_{mix}. Circulation time was determined by analyzing the change in tracer concentration in the zone immediately downstream of the tracer injection point outlet (zone "46" in Fig. 2). The change in tracer concentration as a function of time was periodical, an example graph is shown in Fig. 3. The length of the circulation period was equal to the tracer circulation time. It could be determined from the distance between the maxima of successive peaks of concentration fluctuations, however, the shape of the peaks is not exactly symmetrical, so the distance between the tops of successive peaks was changing. In order to determine the circulation time more accurately, Fourier analysis was employed. Instead of determining the length of the circulation period directly, the frequency of the fluid circulation, f_l, was determined. Frequency analysis was carried out using the Fast Fourier Transform (FFT) algorithm allowed to determine the tracer's circulation frequency with high accuracy. Then, the circulation time could be determined as the inverse of the circulation frequency:

$$\tau = \frac{1}{f_l} \tag{4}$$

where:
τ – tracer circulation period, [s]
f_l – tracer circulation frequency, [1/s]

In order to verify the correctness of the selection of the analyzed segment of the image graph, tests were also carried out for other zones of the image. The results of the tests yielded frequency values consistent with

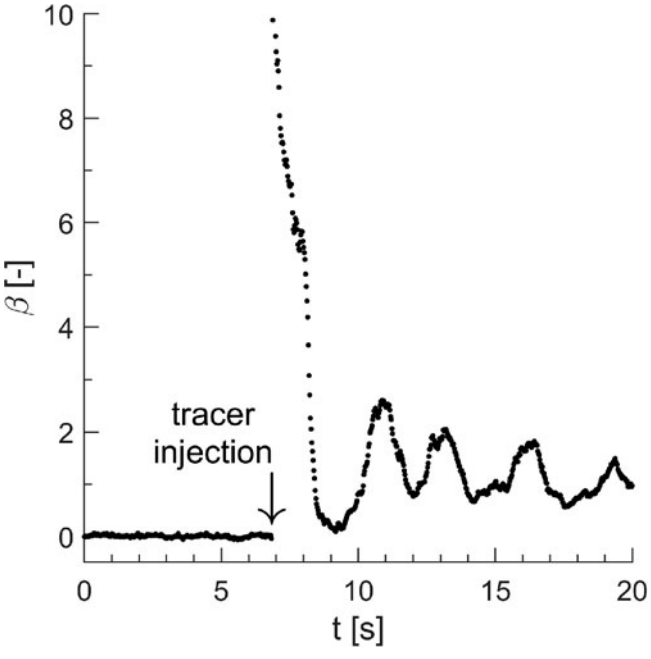

Figure 3. Experimentally determined dimensionless tracer concentration, β, versus time, t, in the zone "46" of investigated HATR for a gas flow rate equal to Q_V/L = 350 dm^3/(h m)

the originally selected area (with the accuracy to the resolution of the frequency spectrum determined using the FFT algorithm); however, the height of the peaks was lower, which could be the result of lower measured concentrations. The obtained circulation time was also consistent with the circulation time estimated based on the distance between consecutive peaks in the graph, further confirming the validity of the selected methodology.

Perfect mixing means a case in which the concentration of all components in a mixture is identical throughout the volume of that mixture. The mixing time, t_{mix}, is called the time required to achieve a certain degree of homogeneity of the mixture. Perfect mixing is theoretically achieved after an infinitely long time, so the mixing time is most often determined for the moment when the local concentration of the tracer at each point in the apparatus deviates by no more than a certain degree (±5% in this work) from the concentration in solution after perfect mixing[8, 12]. The change in tracer concentration at a selected point in the apparatus has a pattern similar to that of a damped harmonic oscillator. When we determined the change in concentration at another point in the apparatus, we would obtain a curve with a similar pattern. The unifying feature of curves depicting the change in tracer concentration at different points on the apparatus is that we can enclose all of these curves between curves that will depict the maximum amplitude of these oscillations over time – the so-called envelope.

The dimensionless tracer concentration, β, takes a value equal to 1 when complete mixing is achieved. If we assume that local changes in tracer concentration will have a time course identical to that of the damped oscillator, the upper envelope can be described by an equation similar to that of the damped oscillator (5)[13]:

$$\beta_{max} = 1 + 2\exp[-b(t - t_0)] \tag{5}$$

where:

$\beta_{\max}(t)$ – maximum dimensionless concentration of the tracer in the apparatus, [–]

b – amplitude decay rate, [1/s]

t – experiment time, [s]

t_0 – tracer injection time, [s]

Equation (5) is an approximation of the envelope of the impulse response function for an apparatus with complete recirculation. A feature of the function described by Equation (5) is that it tends asymptotically to the unity, similar to the true envelope of the impulse response function for a system with recirculation (after normalization performed using Equation (3)). However, it should be noted that the function described by Equation. (5) at the time of the tracer injection ($t = t_0$) takes on a value equal to 3, and the true envelope of the function can take on much larger values. However, the initial part of the curve is not used to determine the mixing time, so using Eq. (5) to determine mixing time does not introduce significant error. Khang and Levenspiel[13] showed that this function reproduces with relatively good accuracy the course of the real envelope of the impulse response function for a system with circulation for low values of the inhomogeneity coefficient, h (e.g. for inhomogeneity of ±5%, h = 0.05). This was also confirmed by Murakami et al.[9], where their paper describes that an exponential function of the general form as in equation (5) can be used to approximate the envelope of the impulse response function with an accuracy of 1% for h<0.4 and therefore for the region that is used to determine the mixing time. Therefore, it was decided to choose Eq. (5) to approximate the envelope of the impulse response function.

Equation (5) describes the upper envelope of the function. When we want to determine the mixing time, we need to determine the time at which the value of the amplitude of the function, a, will be no greater than the specified maximum degree of inhomogeneity. In the literature, the most common value for the degree of inhomogeneity used to determine mixing time is ±5%[10, 11, 14], however, other values are also found, such as ±1%[15] or ±10%[16]. In this study, the degree of inhomogeneity was set to be equal to ±5%.

Assuming that the mixing time is the time when the difference between the maximum local concentration of the tracer in the apparatus was no greater than 5%[8] (β_{max} = 1.05) of the concentration after complete mixing, then after transforming equation (5), we can obtain an expression to calculate the time required to acquire this maximum inhomogeneity, i.e. the mixing time (6):

$$t_{mix} = t - t_0 = \frac{1}{b}\ln 40 \tag{6}$$

In order to determine the envelope of the function experimentally, the tracer concentration distributions as a function of time were determined for multiple points inside the apparatus. The procedure for determining the local concentration was identical to that described earlier. Knowing the impulse response curves at multiple points in the apparatus cross-section, the maximum tracer concentration was selected for each time instant, obtaining points representing the envelope.

Unfortunately, due to the curvature of the apparatus wall, the presence of gas bubbles and fluid surface movements, it was not possible to measure the tracer concentration at all points in the cross section of the apparatus. An example of the experimentally obtained data is shown in Fig. 4. There we can see that there is a certain bend in the course of the experimental points at t = 9 s. It is due to the fact that the area where the tracer concentration was highest was located in the recorded video outside the zones for which the tracer concentration was determined. For this reason, the concentration chosen for analysis was not the highest in the entire apparatus, but the highest among the analyzed zones, so that some of the points do not represent the actual envelope of the function, but are below this envelope.

Experimental points for the time from the tracer injection to the end of the measurement were taken for further analysis. The model presented in equation (5) was fitted to the analyzed points. The fitting was carried out using the regression method in Matlab. Ordinary least squares regression leads to the constants of the assumed mathematical model, for which we obtain the function that best fits all the analyzed points. Unfortunately, if there are outliers in the data, the influence of such points on the model equation can be in many situations significant. The obtained model, according to quantitative indicators, may be the best fit to all analyzed points, but the course of such a model deviates in qualitative terms significantly from the actual trend of

the data. Figure 4 shows the curve fitted using the ordinary least squares method. We can see that initially the experimental points are relatively well reproduced with the fitted curve, but in the further part of the graph the fitted curve strongly deviates from the analyzed points. Because of this, the obtained curve goes asymptotically to unity much faster, and the mixing time determined with it will be underestimated.

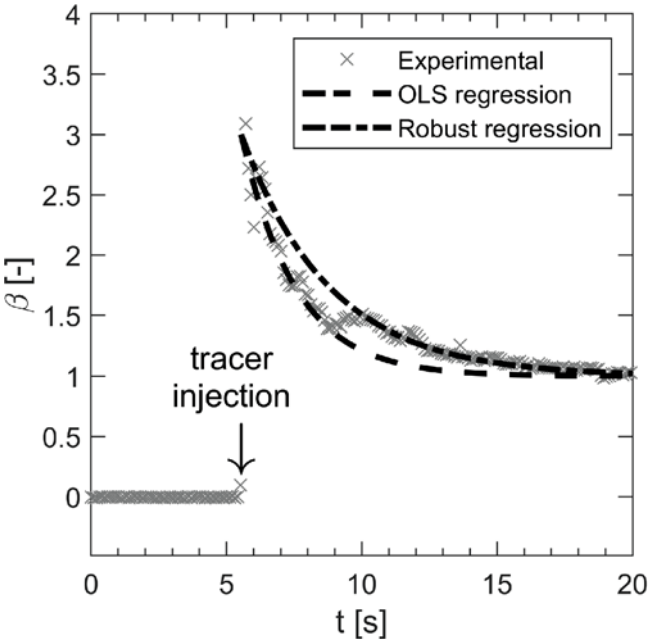

Figure 4. Experimentally determined envelope of dimensionless tracer concentration, β, versus time, t, in the investigated HATR for a gas flow rate equal to Q_V/L = 350 dm^3/(h m). The lines on the graph represent the fit of Equation (5) to the experimental data using ordinary least squares (OLS) regression and robust regression methods

In order to minimize the impact of outliers, it is possible to use robust regression methods[17]. They are modifications of the ordinary least squares method that take into account the weights for each of the analyzed points. Within this work, a bi-square robust regression algorithm was chosen. In the first iteration, this algorithm works like the ordinary least squares method. Then, based on the distance of the points from the fitted curve, the weights for each of the analyzed points are determined. Calculated weights are then taken into account in subsequent iterations of the algorithm. The farther a point is from the fitted curve, the less weight is assigned to it. Thus, such an algorithm is able to automatically detect points that are highly likely to be outliers in the data and minimize their impact on the result of the fit. In Figure 4, we can see the curve that was fitted using robust regression. This curve is a much better representation of the experimental points further down the curve, where the dimensionless concentration approaches unity, that is, where the mixing time is determined.

Robust regression methods produce solutions that, for the data as a whole, have inferior values of fit quality coefficients, such as coefficient of determination (R^2) and root mean squared error (RMSE), however, after taking into account the selected weights for each of the analyzed points, the values of these coefficients often increase significantly. In the case shown in Figure 4., R^2 = 0.87 and $RMSE$ = 0.157 were obtained for the ordinary least squares method, and R^2 = 0.84 and $RMSE$ = 0.195 were calculated for the robust regression method. However, after taking into account the weights selected, these fit quality coefficients took on the values R^2 = 0.99 and $RMSE$ = 0.032. The results of the quality of fit for the other data series were similar. The curves fitted using the robust regression method also took on the expected shape of the envelope of the impulse response function to a much greater extent.

In this paper, the Peclet number for radial dispersion, Pe_r, which is defined as (7), is used as a measure of the intensity of the radial dispersion:

$$\mathrm{Pe}_r = \frac{u_r D_r}{\boldsymbol{D_r}} \tag{7}$$

where:
Pe_r – Peclet number for radial dispersion, [–]
u_r – liquid flow velocity, [m/s]
D_r – pipe diameter, [m]
$\boldsymbol{D_r}$ – radial dispersion coefficient, [m^2/s]

At this point, it should be noted that the nomenclature of the dimensionless modulus represented by the right-hand side of equation (7) is not consistent in the literature. Some authors here use the name Bodenstein number[3], and the inverse of this modulus is also called the dispersion number[2].

As pointed out by many authors, the value of the dimensionless Pecelt number for systems with circulation (such as loop apparatuses or mixers) is dependent on the circulation time and on the mixing time. This relationship was also analyzed in an earlier work[12]. In that paper, the following relationship was demonstrated (8):

$$\mathrm{Pe} = \frac{1}{a}\frac{t_{mix}}{\tau} \tag{8}$$

where:
a – constant, [–]

Thus, knowing the values of circulation time and mixing time, the value of the Peclet number can be determined.

All tests were conducted depending on the flow rate of gas introduced into the apparatus, Q_V. A more appropriate way of expressing the gas flow in this case is to express the flow rate related to the length of the aeration zone, L. The present study investigated the effect of aeration density in the range of Q_V/L = 100÷350 $L/(h\ m)$. The selected range of flow rates was given by the limitations of the test stand. The lower limit of this range was selected due to the lowest possible gas flow rate that ensured uniform operation of the gas distributor, and the upper limit was based on the maximum achievable gas flow rate in the apparatus. Few reports can be found in the literature regarding axial mixing in HATR. In his work, Moser[3] studied the effect of gas flow rates in the range of Q_V/L=25÷125 $L/(h\ m)$, a range that partially overlaps with the range of gas flow rates in the present work. Unfortunately, no work regarding radial mixing was found.

Uncertainty analysis

The uncertainty in the measurement of the circulation frequency, f_l, was estimated based on the resolution of the frequency determined using the Fast Fourier Transform (FFT) algorithm. The frequency resolution

was dependent on the length of the analyzed portion of the video; however, increasing the length of the analyzed video sequence would lead to a situation where a significant portion of the video would be an image of a completely mixed liquid. This, in turn, could lead to a reduction in the intensity of the peaks in the power spectrum plot as a function of frequency caused by the circulation of the tracer in the apparatus. As a result, the determined uncertainty of the circulation time was within $\pm(0.20 \div 0.8)$ *s*.

The uncertainty of the constant in equation (4), which was then used to determine the mixing time, t_{mix}, had a small value as a result of the relatively good fit of the envelope model to the experimental data, but given the repeatability of the acquired results and based on a visual determination of the quality of the fit of the obtained curves to the experimental data, the uncertainty of the mixing time measurement was assumed to be equal to ± 1 *s* for all measurements.

It was assumed that the uncertainty of the volumetric gas flow rate setting was equal to the smallest elementary division of the rotameter used, which was 10 dm^3/h.

The uncertainties of indirect measurements were determined using the method of uncertainty propagation for functions of multiple independent variables, which in general form can be written as (9)[18]:

$$\delta f(x_1, x_2, \dots, x_n) = \sqrt{\sum_{i=1}^{n} \left(\frac{\partial f(x_1, x_2, \dots, x_n)}{\partial x_i} \delta x_1 \right)^2} \qquad (9)$$

where:
$f(x_1,x_2,\dots,x_n)$ – arbitrary function of multiple variables
x – dependent variable
δ – uncertainty of variable or function.

RESULTS AND DISCUSSION

Circulation time

The results showing the relationship of circulation time, τ, as a function of aeration density, Q_V/L, are shown in Figure 5. The results presented show a clear tendency. A power regression model (10) was fitted to the experimental data shown in Fig. 5, and the determination coefficient value of 0.847 suggests a good fit of the power model to the data.

$$\tau = 59.5(Q_V/L)^{-0.52} \qquad (10)$$

Unfortunately, no correlations associating circulation time and gas flow rate were found in the literature. Power regression models are often used in describing the circulation velocity as a function of gas flow rate or gas flow velocity in apparatuses with aeration, such as airlift[19], which confirms the validity of the choice of regression model form.

Unfortunately, no correlations associating circulation time and gas flow rate or at least experimental measurement results of circulation time in horizontal tubular reactors with aeration have been found in the literature, so it is not possible to compare the obtained results with other experimental work.

The measured circulation times were in the range of $\tau = 3 \div 6.5$ *s*. When analyzing the effect of circulation

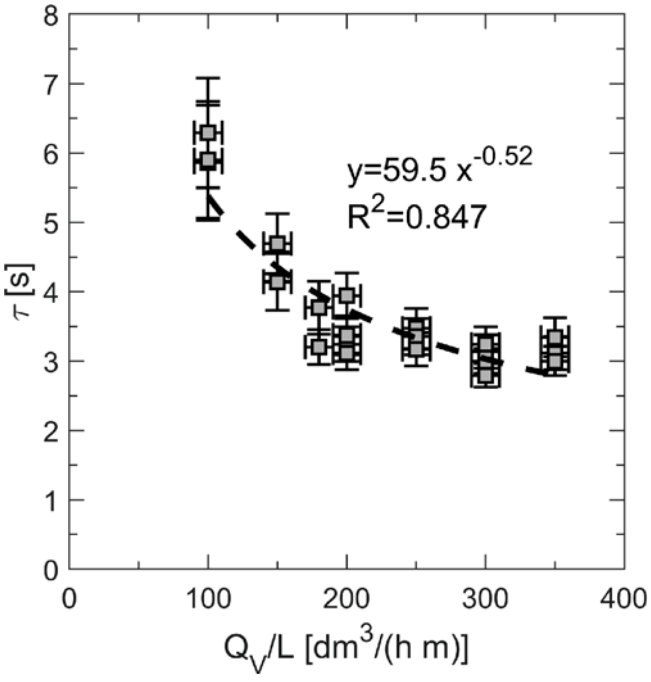

Figure 5. Circulation time, τ, versus air flow rate related to the unit length of investigated HATR, Q_V/L

time on aeration conditions, we must take into account such parameters of the microbiological process as the microbial reaction rate and residence time in the reactor. Microbiological processes are characterized by a much lower rate than chemical processes, and the residence time in microbiological reactors is usually several to even tens of hours. Thus, circulation times on the order of a few seconds should not noticeably affect the course of the microbiological reaction, and with no dead zones in the apparatus, the phenomenon of hypoxia should not be an issue.

We can see that the circulation time decreases with increasing aeration density, however, for Q_V/L in the range of $250 \div 350$ $dm^3/(h\ m)$ the circulation time changes only slightly, in contrast to the results obtained for lower aeration densities. Radial circulation in the apparatus is induced secondarily by gas bubbles rising in the water layer. The liquid on the interfacial surface is carried along with the flowing gas bubble, and viscous friction causes the flow of adjacent liquid layers located deeper in the apparatus, resulting in liquid circulation.

For lower gas flow rates, the diameter of the gas bubbles that form depends mainly on the gas distributor orifice diameter, and the effect of increasing gas flow rate on bubble diameter is marginal. In this case, increasing the flow rate mainly affects the frequency of bubble formation, and only marginally affects the diameter of the bubbles. When the gas flow rate at the distributor orifice is high enough, the gas stream inertia is mainly responsible for the diameter of the bubbles that form. In such a situation, as the flow rate increases, bubbles of increasing diameter are formed, but the frequency of their formation changes only slightly, as was observed during experiments. This coincides with observations made during the experiments, where for flow intensities from $Q_V/L = 250$ $dm^3/(h\ m)$ the observed diameter of the formed gas bubbles was clearly larger than for lower flow rates.

Unfortunately, direct measurement of gas bubble diameters could not be carried out due to the rather

high curvature of the pipe wall, making the image of the bubbles highly warped. In addition, during measurements, adjacent gas bubbles often overlapped, which posed a problem in determining the diameters of individual gas bubbles, since two overlapping bubbles could be treated as one large diameter bubble. However, the size of the bubbles and the frequency of their formation can be estimated based on models available in the literature. The diameter of gas bubbles can be calculated using the bubble formation model proposed by Gaddis and Vogelphol[20], which takes into account not only the physicochemical parameters of the fluid during bubble formation, but also the inertial effects caused by the flow of the gas stream (11):

$$d_b = \left[\left(\frac{6d\sigma_l}{\rho_l g}\right)^{\frac{4}{3}} + \frac{81\mu_l Q_{Vg,o}}{\pi\rho_l g} + \left(\frac{135Q_{Vg,o}^2}{4\pi^2 g}\right)^{\frac{4}{5}}\right]^{\frac{1}{4}} \quad (11)$$

where:
d_b – bubble diameter, $[m]$
d – orifice diameter, $[m]$
σ_l – liquid surface tension, $[N/m]$
ϱ_l – liquid density, $[kg/m^3]$
μ_l – liquid dynamic viscosity coefficient, $[Pa\ s]$
$Q_{Vg,o}$ – gas flow rate in a single orifice, $[m^3/s]$
g – gravitational acceleration, $\left[\frac{m}{s^2}\right]$

Knowing the diameter of the gas bubbles and assuming that they are spherical in shape, we can calculate the volume of the gas bubble, V_b, using equation (12):

$$V_b = \frac{\pi}{6} d_b^3 \quad (12)$$

Then, knowing the volume of a single gas bubble and the volumetric flow rate of the gas in a single distributor orifice, we can calculate the frequency of gas bubble formation, f_b, using equation (13):

$$f_b = \frac{Q_{Vg,o}}{V_b} \quad (13)$$

A graphical representation of the dependence of the frequency of liquid circulation, f_l, as a function of the frequency of gas bubble formation, f_b, can be found in Figure 6. We can see that the relationship between these parameters has a strong linear correlation (coefficient of determination determination $R^2 = 0.83$). This confirms the thesis that the frequency of fluid circulation (and therefore the speed of this circulation) depends more on the number of gas bubbles formed than directly on the amount of gas being conducted.

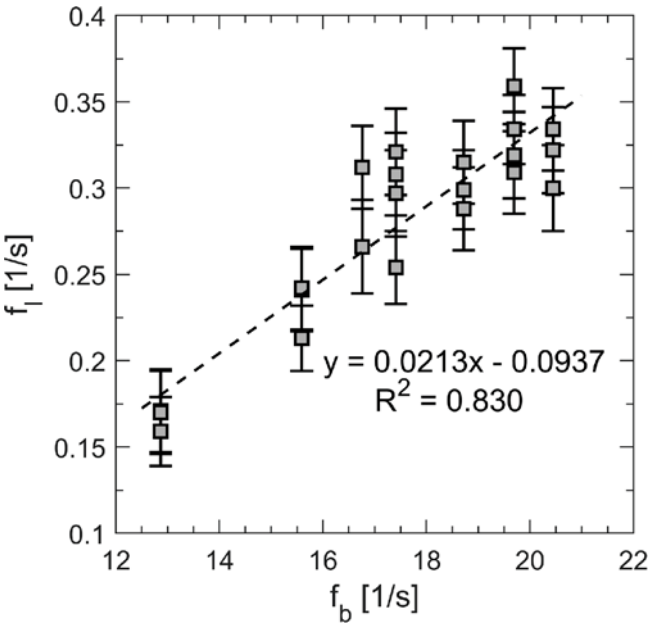

Figure 6. Liquid circulation frequency, f_l, versus calculated bubble formation frequency, f_b

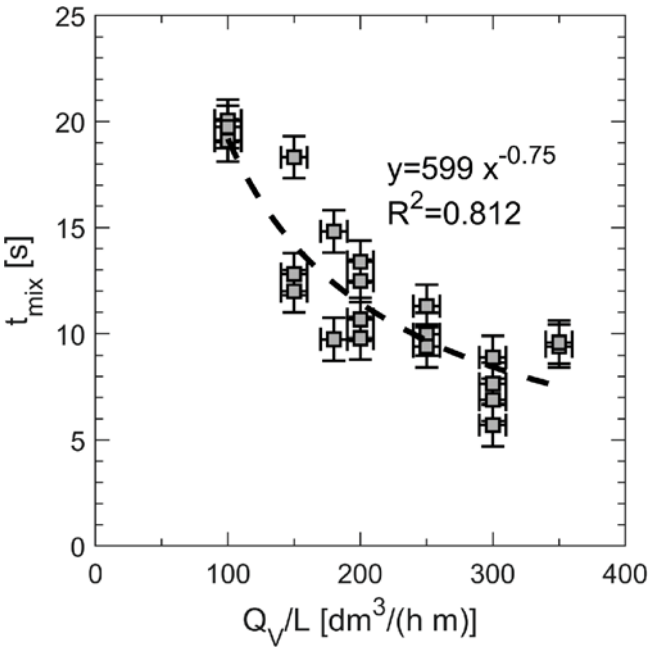

Figure 7. Mixing time, t_{mix}, versus air flow rate related to the unit length of investigated HATR, Q_V/L

Mixing time

The results showing the dependence of mixing time, t_{mix}, as a function of aeration density, Q_V/L, are shown in Figure 7. As for circulation time, a power regression model was fitted to the experimental data (14).

$$t_{mix} = 599(Q_V/L)^{-0.75} \quad (14)$$

Again, no experimental results for measuring radial mixing time and correlations binding mixing time to gas flow rate were found in the literature, but models of similar form are used to describe mixing time as a function of superficial gas velocity in airlift reactors[11]. Due to the more complex nature of the methodology for determining mixing time, the results exhibit greater scatter. However, a general trend showing a decrease in mixing time as a function of gas flow rate is evident, similar to that for circulation time. Also identical to the case of circulation time, we can observe that for gas velocities from $Q_V/L = 250\ dm^3/(h\ m)$ the variation of mixing time is increasingly smaller with the change of gas flow rate.

The air bubble layer significantly reduced mixing between the two sides of the HATR, but did not entirely stop it. The introduction of the tracer on only one side of the apparatus, in addition to the mixing of the tracer with the fluid on the same side, also caused slow mixing of the tracer with the fluid on the opposite side of the bubble layer, so that the concentration of the tracer was slowly reduced as the experiment continued,

which resulted from the mixing of the fluid on both sides of the apparatus. This effect was minimized by symmetrically introducing the tracer on both sides of the gas bubble layer.

3.3. Radial dispersion

The Peclet number, which is a measure of the intensity of mixing in the apparatus, can be determined using Equation (8). The value of the constant of Equation (8) depends directly on the value of the degree of inhomogeneity adopted when determining the mixing time. A mathematical equation binding together the constant from the Eq. (8) and the degree of inhomogeneity, h, based on a theoretical model of dispersive flow with total recirculation can be found in Blenke[21] (15):

$$a = \frac{0.692 - \ln h}{39.48} \tag{15}$$

We can find an equation of similar form in the work of Murakami et al.[9] (16):

$$a = \frac{-\ln\left(\frac{h}{2}\right)}{4\pi^2} \tag{16}$$

The values of the constant calculated using equations (15) and (16) for the degree of inhomogeneity assumed in this article of ±5% ($h = 0.05$) are identical and equal to $a = 0.0934$ ($1/a = 10.7$) for both equations. Thus, we can see that the value of the constant a depends only on the chosen degree of inhomogeneity, h, so the values of the mixing time determined for different values of the degree of inhomogeneity will be proportional to each other. In the final analysis, this means that the choice of the degree of inhomogeneity is motivated mainly by the convenience of the experimenter. Relatively high selected values of the degree of inhomogeneity can result in short mixing times, so in the case of fast mixing and low frequency of measurements, the obtained mixing times may be subject to high uncertainty. When very low values of h are selected, the determination of mixing time can be problematic for measurements subject to high values of measurement noise.

The theoretical values of the coefficient a determined by Blenke[21] and Murakami et al.[9] were also confirmed experimentally. Verlaan et al.[10] in his work studied mixing in an airlift reactor. Such an apparatus can be taken as a good example of a complete circulation system. Based on measurements of mixing time, circulation time and by determining the Peclet number for the apparatus, they demonstrated that the quotient of mixing time for a degree of inhomogeneity of +5% and circulation time (also called dimensionless mixing time) is proportional to the value of the Peclet number. Obtained coefficient was equal to $a = 0.093$ ($1/a = 10.8$). Similar results, also for the airlift apparatus, can be found in the paper by Sánchez Mirón et al.[14], who obtained experimentally a coefficient $a = 0.104$ ($1/a = 9.6$). Also in earlier work, the value of the coefficient was confirmed experimentally[12] ($a = 0.0934$, $1/a = 10.7$).

Research on mixing time was also conducted by Khang and Levenspiel[13], who investigated mixing in agitated vessels. In their work, they used tanks-in-series model with recirculation to describe mixing. Considering the relationship associating the number of theoretical tanks with complete mixing, N, with the Peclet number[2] (17):

$$Pe = 2N \tag{17}$$

The model obtained by the authors has an identical form to the model proposed by Murakami et al.[16]. In their work, Khang and Levenspiel also experimentally confirmed the derived model[13].

Given that similar theoretical models have been derived for different types of apparatus (loop reactors and stirred tanks), for the cases of one- and two-phase flow, and that they have received experimental confirmation, we can conclude that these models should be valid for any case where we are dealing with dispersive flow. Dispersive flow itself can be described using the dispersion coefficient by means of similar mathematical relations as flow with diffusion. Also like diffusion, the value of the dispersion coefficient does not depend on the direction of the fluid flow[2]. These assumptions therefore imply that the mechanism of dispersion flow in the axial and radial directions can be described by the same mathematical models. In summary, the model assumptions for axial dispersion should also be valid for the case of radial dispersion, which allows the use of models describing axial flow with dispersion to describe radial flow with dispersion. Thus, equation (8) can also be used to estimate the Peclet number for radial dispersion.

The values of the Peclet number for radial dispersion, Pe_r, as a function of aeration density, Q_V/L, are shown in Fig. 8. If the values of the Peclet number is lesser than 0.1, such a flow can be treated with a good approximation as a flow with ideal mixing, while for values of the Peclet number above 20 the dispersive flow can be approximated with a plug flow model with reasonable accuracy[22]. We can note that the obtained values of the Peclet number fluctuate in the range of 20÷45. This means that the circulating fluid flow can be approximated using simpler model of plug flow.

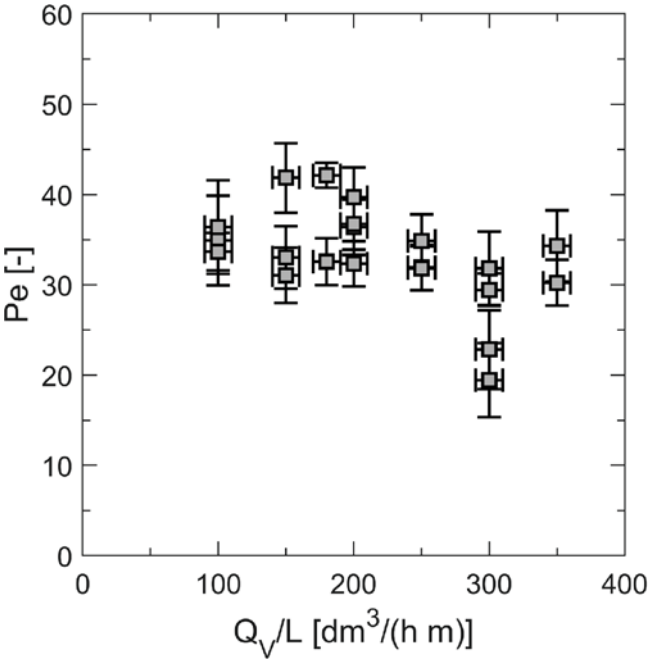

Figure 8. Peclet number, Pe, versus air flow rate related to the unit length of investigated HATR, Q_V/L

CONCLUSIONS

Tracer studies using a color tracer allowed obtaining the circulation time and mixing time for radial circulation in the *horizontal aerated tubular reactor* (HATR) studied. The tracer concentration was measured using

a non-invasive optical method. The tests were carried out over a range of gas flow rates per unit length equal to $Q_V/L = 100 \div 350\ dm^3/(h\ m)$.

The circulation time was determined based on Fourier analysis of the time series of the impulse response at a selected point in the cross-section of the apparatus. Under the experimental conditions, the determined circulation time was in the range of $\tau = 3 \div 6.5\ s$. The circulation time also decreased with increasing gas phase flow rate, however, for gas flow rates starting from $Q_V/L = 250\ dm^3/(h\ m)$ the value of circulation time changed only slightly.

The frequency of fluid circulation was compared with the calculated frequency of gas bubble formation. The results of the comparison, shown in Figure 6, indicate a strong linear correlation between these frequencies. This may suggest that the frequency of liquid circulation (and therefore the circulation velocity) is affected more by the number of gas bubbles formed than by the gas phase flow rate itself.

The determined mixing time was in the range of $t_{mix} = 5 \div 20\ s$. The value of the determined mixing time was subject to high uncertainty, but the general trend in the change of mixing time as a function of gas phase volume flow was identical to that of circulation time - mixing time decreased with increasing gas flow.

The Peclet number for radial dispersion, which characterizes the degree to which the stream structure deviates from plug plow, was determined based on an equation relating it to circulation time and mixing time. The obtained values of the Peclet number are in the range $Pe_r = 20 \div 45$ indicate that the structure of the radial flow deviates significantly from the complete mixing and may be approximated rather using plug flow model than ideal mixing. This means that the concentration field of substances introduced pointwise into the apparatus becomes uniform only after some time. In cases where the regulation of the pH of the medium in the reactor is carried out by the addition of highly concentrated solutions of strong alkalis or strong acids, such a situation may be undesirable, as it can lead to the demise of microorganisms by putting the cells in contact for too long with a fluid with a pH significantly different from that recommended for the microorganisms being cultured.

SUMMARY

– Mixing time was successfully determined using Fourier analysis of the tracer impulse response curves.

– Mixing frequency (inverse of mixing time) is strongly dependent on the frequency of formation of new gas bubbles on the gas distributor.

– The determined mixing time is in the range of $t_{mix} = 5 \div 20\ s$.

– The values of the Peclet number for radial circulation ($Pe_r = 20 \div 45$) suggest that such flow can be treated rather as plug flow than ideal mixing.

LITERATURE CITED

1. Šantek, B., Ivančić, M., Horvat, P., Novak, S. & Marić, V. (2006). Horizontal tubular bioreactors in biotechnology. *Chem. Biochem. Engin. Quarterly*, 20(4), 389–399. DOI: 10.15255/CABEQ.2014.445.

2. Levenspiel, O. (2011). *Tracer technology: modeling the flow of fluids* (Vol. 96). New York, USA: Springer Sci. & Business Media.

3. Moser, A. (1991). Tubular bioreactors: case study of bioreactor performance for industrial production and scientific research. *Biotechnol. Bioengin.*, 37(11), 1054–1065. DOI: 10.1002/bit.260371111.

4. Levenspiel, O. (2011). *Chemical reaction engineering*. New York, USA: John Wiley & Sons.

5. Borchardt, J.A. (1971). Biological waste treatment using rotating discs. *Biological Waste Treatment*, 131–140.

6. Gorbach, G. (1969). Die kontinuierliche Dünnschichtfermentation. *Fette, Seifen, Anstrichmittel*, 71(2), 98–103.

7. Rossi, D., Gargiulo, L., Valitov, G., Gavriilidis, A. & Mazzei, L. (2017). Experimental characterization of axial dispersion in coiled flow inverters. *Chem. Engin. Res. Design*, 120, 159–170.

8. Essadki, A.H., Gourich, B., Vial, C. & Delmas, H. (2011). Residence time distribution measurements in an external-loop airlift reactor: Study of the hydrodynamics of the liquid circulation induced by the hydrogen bubbles. *Chem. Engin. Sci.* 66(14), 3125–3132. DOI: 10.1016/j.ces.2011.02.063.

9. Murakami, Y., Hirose, T., Ono, S. & Nishijima, T. (1982). Mixing properties in loop reactor. *J. Chem. Engin. Japan*, 15(2), 121–125. DOI: 10.1252/jcej.15.121.

10. Verlaan, P., Van Eijs, A.M.M., Tramper, J., Van't Riet, K. & Luyben, K.C.A. (1989). Estimation of axial dispersion in individual sections of an airlift-loop reactor. *Chem. Engine. Sci.* 44(5), 1139–1146. DOI: 10.1016/0009-2509(89)87013-7.

11. Gavrilescu, M. & Tudose, R.Z. (1997). Mixing studies in external-loop airlift reactors. *Chem. Engin. J.* 66(2), 97–104. DOI: 10.1016/S1385-8947(96)03177-4.

12. Prończuk, M. & Bizon, K. (2019). Investigation of the liquid mixing characteristic of an external-loop hybrid fluidized-bed airlift reactor. *Chem. Engin. Sci.* 210, 115231. DOI: 10.1016/j.ces.2019.115231.

13. Khang, S.J. & Levenspiel, O. (1976). New scale-up and design method for stirrer agitated batch mixing vessels. *Chem. Engin. Sci.* 31(7), 569–577. DOI: 10.1016/0009-2509(76)80020-6.

14. Sánchez Mirón, A., Cerón García, M.C., García Camacho, F., Molina Grima, E. & Chisti, Y. (2004). Mixing in bubble column and airlift reactors. *Chem. Engin. Res. Design*, 82(10), 1367–1374. DOI: 10.1205/cerd.82.10.1367.46742.

15. Lechowska, J., Kordas, M., Konopacki, M., Fijałkowski, K., Drozd, R. & Rakoczy, R. (2019). Hydrodynamic studies in magnetically assisted external-loop airlift reactor. *Chem. Engin. J.* 362, 298–309. DOI: 10.1016/j.cej.2019.01.037.

16. Onken, U. & Weiland, P. (1980). Hydrodynamics and mass transfer in an airlift loop fermentor. *Europ. J. Appl. Microb. Biotech.* 10, 31–40. DOI: 10.1007/BF00504725.

17. Andersen, R. (2008). *Modern methods for robust regression* (No. 152). Sage.

18. Taylor, J. (1997). Introduction to error analysis, the study of uncertainties in physical measurements (2nd ed.). Sausalito, California, USA: University Science Books.

19. Chisti, M.Y., Halard, B. & Moo-Young, M. (1988). Liquid circulation in airlift reactors. *Chem. Engin. Sci.* 43(3), 451–457. DOI: 10.1016/0009-2509(88)87005-2.

20. Gaddis, E.S. & Vogelpohl, A.J.C.E.S. (1986). Bubble formation in quiescent liquids under constant flow conditions. *Chem. Engin. Sci.* 41(1), 97–105.

21. Blenke, H. (1979). Loop reactors. *Adv. Biochem. Engin.* vol 13, 121–214). DOI: 10.1007/3540094687_8.

22. Chisti, Y. (1989). Airlift Bioreactors. New York, USA: Elsevier.